Circumglobal Teleconnections, the Jet Stream Waveguide, and the North Atlantic Oscillation

GRANT BRANSTATOR

National Center for Atmospheric Research, Boulder, Colorado*

(Manuscript received 3 September 2001, in final form 7 February 2002)

ABSTRACT

Monthly and seasonally averaged upper-tropospheric Northern Hemisphere winter fields are examined to determine whether the waveguiding effect of the time-averaged tropospheric jets on low-frequency disturbances that is predicted by theory does affect the behavior of these disturbances. It is found that, indeed, disturbances in the vicinity of the mean jets, particularly the jet that stretches across South Asia, are fundamentally different from those that reside in regions where the mean winds have weaker meridional gradients, like the mid-Pacific. Patterns of variability in the jets tend to be smaller scale and to consist of zonally oriented chains of anomalies while variability in the mid-Pacific is composed of patterns with distinct meridional orientation. Because they are meridionally trapped and zonally elongated, patterns associated with the jet stream waveguide connect activity at points that are much farther apart than do patterns in other regions of the globe.

Within the South Asian waveguide, variability tends to be composed of a zonal wave-5 feature with no favored longitudinal phase. One phase of this pattern is special in that it covaries with distant regions in midlatitudes producing a pattern of variability that circumscribes the hemisphere. This special pattern has a noticeable zonal mean component. Furthermore, it is prominent enough that for the upper troposphere it is embedded in the leading EOF of streamfunction and is essentially the same as the leading EOF of the v wind component. Over the North Atlantic, its structure has a great deal in common with the structure of the North Atlantic Oscillation, so that its features can make significant contributions to plots of hemispheric circulation anomalies associated with that phenomenon.

1. Introduction

The atmospheric teleconnection patterns that have had the largest impact on atmospheric scientists' thinking about variability on interannual and longer timescales are made up of chains of lobes whose centers are connected by lines that have prominent meridional components. The Pacific–North American pattern (Wallace and Gutzler 1981), the North Atlantic Oscillation (Walker and Bliss 1932; Hurrell 1995), and the Tropical North American pattern associated with equatorial Pacific heating anomalies (Barnston and Livezey 1987) all have this characteristic. The pronounced meridional character of these patterns goes hand in hand with the impression that each pattern is confined to a longitudinal sector of the globe. Indeed the assumption that patterns of low-frequency variability are fundamentally regional has been held with such confidence that many studies that seek to identify the basic patterns of variability intentionally build in a bias toward regionality by either analyzing only one sector of the globe at a time [as, e.g., in Kimoto and Ghil (1993)] or by using varimax rotated empirical orthogonal functions [as, e.g., in Horel (1981) and Barnston and Livezey (1987)].

Recently, more emphasis on the global, or at least hemispheric, character of one of these teleconnection patterns has been pointed out. Thompson and Wallace (1998) have concluded that the North Atlantic Oscillation is actually a regional depiction of what is fundamentally a hemisphere-wide pattern, which they have dubbed the Arctic Oscillation. The Arctic Oscillation appears to achieve its global character from a prominent zonal mean component and for this reason is sometimes referred to as an annular mode. But as explained in the following paragraphs, theory suggests there could be a second means of producing low-frequency teleconnections between very widely separated points, namely the trapping and focusing effects of the time-mean tropospheric jets as they act as waveguides. These effects would not produce zonal mean anomalies but rather zonally oriented chains of perturbations. In this paper we analyze low-frequency behavior in GCMs and in nature to see whether distant, nonannular teleconnec-

* The National Center for Atmospheric Research is sponsored by the National Science Foundation.

Corresponding author address: Dr. Grant Branstator, National Center for Atmospheric Research, P.O. Box 3000, Boulder, CO 80307-3000.
E-mail: branst@ucar.edu.

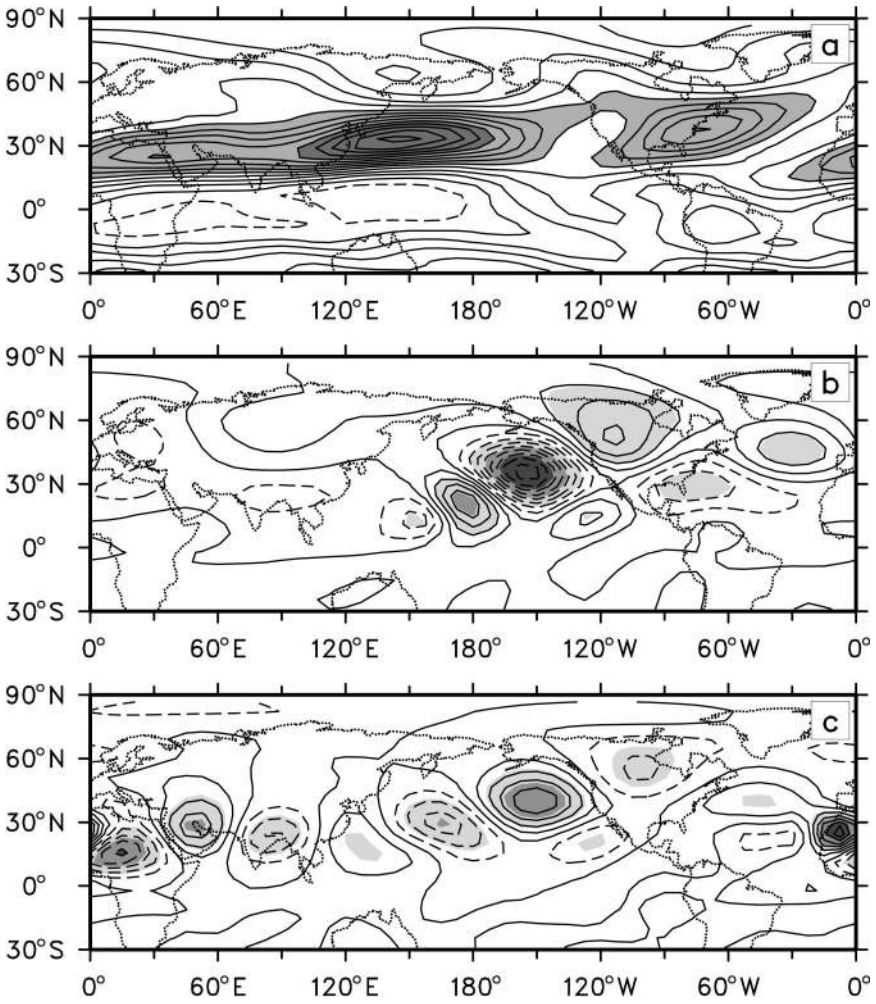

FIG. 1. (a) Climatological average 300-mb nondivergent u wind component for DJF based on 39 reanalysis winters. Contour interval: 5 m s^{-1}. (b) Streamfunction response of the barotropic vorticity equation linearized about mean 300-mb streamfunction for the same dataset used in (a) and forced by a vorticity source centered at (25°N, 165°E). Contour interval: 1.5×10^{-6} m^2 s^{-1} c) Same as (b) with forcing at (25°N, 15°W). Contour interval: 0.75×10^{-6} m^2 s^{-1}. Here and elsewhere negative contours are dashed.

tions do occur and whether they have the signatures expected for perturbations under the waveguiding influence of the jets.

Since Longuet-Higgins's (1964, 1965) and Hoskins et al.'s (1977) investigations of rays on the sphere, the prominent meridional component of dispersing Rossby–Haurwitz waves has been recognized. However, once the refractive effects of a zonally symmetric background wind field are taken into account it becomes apparent that low-frequency circulation anomalies of intermediate scale will tend to be confined to latitudes where the tropospheric jet is centered. For example, Hoskins and Karoly's (1981) analysis of the so-called stationary wavenumber for such a state implies that stationary waves with total wavenumber of about six will be meridionally trapped near 30°N, where the core of the zonal mean jet resides. Of course, as shown in Fig. 1a, the winter jet in nature is not zonally symmetric. Rather it is concentrated in swaths that extend from South Asia to the western Pacific and across the North Atlantic. Branstator (1983), considering linear solutions of the nondivergent barotropic vorticity equation with a background state that was longitudinally nonuniform, found that trapping of the sort suggested by Hoskins and Karoly's stationary wavenumber analysis would also occur in jets that are longitudinally confined provided the jet is of sufficient zonal extent. On the other hand, he found that in regions devoid of meridional gradients (Hoskins et al. 1977), arching structures in which meridional group velocities were pronounced were the norm. Hence, depending on where a low-frequency disturbance forms relative to the background state, its meridional structure will be very different.

Branstator's study, and a more comprehensive anal-

ysis done by Hoskins and Ambrizzi (1993), showed that the contrasting behavior could be interpreted in terms of a Wentzel-Kramer-Brillouin (WKB)–based refractive index that was a function of the local background state. This analysis indicates that disturbances near the jet core will be refracted toward the core, meaning that the jet acts as a waveguide. In addition to producing disturbances that are structurally different from ones that occur in the absence of a jet, linear solutions in those papers suggest that the waveguide action of the jet has the potential to enhance the geographical extent of low-frequency perturbations. Since the disturbances are meridionally confined, their energy is not dispersed over as broad a region and is able to propagate farther before being dissipated. The tendency for more extensive zonal energy propagation is further enhanced by the fact that the group velocity is proportional to the background winds, which are especially strong in the jet.

Figure 1c displays a solution to the barotropic vorticity equation that demonstrates these attributes of low-frequency disturbances under the influence of the South Asian jet. To produce this solution[1] the model is linearized about December–February mean 300-mb streamfunction and forced at (25°N, 15°W), just upstream of the Asian jet. The zonal elongation and lack of meridional extent of this response is especially noticable when compared to the solution in Fig. 1b, which was produced by a source at (25°N, 165°E). In that case, where the influence of background jets is minimal, the more familiar arching response results.

In spite of the possibility of there being patterns of variability that are largely meridionally trapped, there has been a natural tendency for observational studies to focus on patterns with marked meridional orientation. Most studies tend to concentrate on the northern oceanic basins because this is where low-frequency variability is most prevalent (Blackmon 1976). But as Fig. 1a and the above solutions suggest, these are the regions where patterns with meridional orientation are expected to dominate. On the other hand some studies that have looked beyond these regions have noticed evidence of zonally oriented perturbation chains in the vicinity of mean jets. Using lag-correlation analysis that picks out features undergoing slow phase propagation, Kiladis and Weickmann (1992), Hsu and Lin (1992), and Ambrizzi et al. (1995) have all found evidence of such features.

Motivated by the above theory and observational studies, we begin our examination of whether low-frequency disturbances under the influence of the jet stream waveguide are structurely distinct from those that do not feel its effects and whether the waveguide can lead to covariability between widely separated points without recourse to annular anomalies. We start with a description of the datasets we will study.

2. Datasets and statistical significance

Part of our study consists of analyzing fields produced by the National Centers for Environmental Prediction–National Center for Atmospheric Research (NCEP–NCAR) reanalysis project (Kalnay et al. 1996). We have used global fields from December, January, and February for the 39 Northern Hemisphere winters between December 1958 and February 1997, and the fields have been truncated rhomboidally to total wavenumber 15 (R15) by using a spherical harmonic basis.

Ideally we would like to draw all of our conclusions from these observational fields, but as in all investigations of the structure of seasonal and longer timescales, the short data record from nature raises questions about the confidence one can have in such results. Moreover, we would like to examine the effects of the jets on the full range of low-frequency disturbances generated by the atmosphere, but any statistical analysis of monthly or seasonal averages in nature may tend to be so influenced by the atmospheric response to tropical Pacific sea surface temperatures (SSTs) that this will not happen. To deal with these difficulties, we employ two strategies. First, when analyzing the observational data, rather than use monthly or seasonal averages, we use monthly mean departures from centered 3-month averages. This has the effect of at least crudely removing the influence of interannual variations in SSTs. It also removes the effects of trends and increases the sample size from what we would have if we used seasonal means. Second, before considering nature we analyze ensemble integrations of atmospheric general circulation models. As explained by Leith (1978), by using ensembles we can remove the effects of interannually varying SST, and we can analyze much larger samples than are available for nature thus leading to high confidence in the results. Furthermore, if it turns out that our results for nature are similar to those for the highly reliable GCM data, then our confidence in the representativeness of the observational results will be enhanced.

The model-generated data we have analyzed are a 22-member ensemble simulated by Community Climate Model 3 (CCM3) of the National Center for Atmospheric Research and a nine-member ensemble produced by the National Aeronautics and Space Administration (NASA) Seasonal-to-Interannual Prediction Project (NSIPP) atmospheric general circulation model. CCM3 is an up-to-date model whose properties have been described by Kiehl et al. (1998), Hack et al. (1998), and Hurrell et al. (1998). The CCM3 ensemble members are forced by sea surface temperatures observed from

[1] In this calculation the model is identical to the one used in Branstator (1985) except it is damped with a characteristic time of 4 days and the basic state is based on December–February from the reanalysis dataset described in section 2. Forcing consists of a steady vorticity source with central value of 1×10^{-5} s^{-1} day^{-1}, which decreases linearly until it reaches a distance of 1.5×10^{6} m, where it vanishes.

December 1950 through November 1994. Ten of the ensemble members utilize SSTs from the Global Sea Ice and SST version 2 (GISST2) dataset (Rayner et al. 1996), five use SSTs produced at NCEP using EOF reconstruction (Smith et al. 1996), and seven use SSTs that are a combination of NCEP reconstructed SSTs before 1982 and SSTs analyzed via optimum interpolation after 1982 (Reynolds and Smith 1994). We have judged the SSTs to be similar enough on the timescales of interest (Hurrell and Trenberth 1999) to warrant the combining of the experiments into a single ensemble. The NSIPP model has been recently developed and tested at NASA, and its properties are described by Bacmeister et al. (2000). The experiments we examine use GISST observed SSTs before 1982 and optimum interpolation SSTs after 1982, and we use those portions of integrations that correspond to January 1951 through December 2000. For ensembles from both GCMs we truncate the fields to R15 and analyze departures from ensemble averages, thus approximately restricting our results to the internal variability of the system. Unlike for observations from nature, the length of these datasets makes it unnecessary to maximize the sample size, so we consider December–February, rather than monthly, averages as a superior method of focusing on low frequencies.

To appreciate the value of using the model ensembles it is worth briefly comparing the heightened confidence we have when analyzing their behavior compared to the confidence we have when considering the record from nature. For the most part our study centers on correlations between temporal variability at pairs of points on the globe. As explained in the appendix, for a given dataset, errors bars on correlation coefficient estimates are a function of the value of the estimate. But for the purpose of comparing datasets it is sufficient to note that for our CCM3 ensemble the half-width of 95% confidence intervals is about 0.05 and for the NSIPP ensemble it less than 0.10, while for the shorter reanalysis dataset it is about 0.20.

3. GCM results

a. Analysis of 300-mb streamfunction

We begin our analysis by considering the December–January–February (DJF) seasonal mean 300-mb streamfunction from CCM3, the largest dataset in our study. We choose to focus on streamfunction rather than geopotential heights because we are especially interested in behavior in the vicinity of the South Asian mean jet and hence do not wish to use a field whose variance is automatically diminished at low latitudes. We want to learn about the structure of anomalies in these fields as a function of geographical position. To do this we use one-point correlation maps that chart the temporal correlation between variability at a base point and variability at every other point on the globe. As anticipated, when we examine charts for base points in South Asia and in the central North Pacific, we do find very different signatures. Figure 2a shows the plot for the (24°N, 172°W) base point, a representative example for a North Pacific location. We see the structure consists of an arching pattern with significant meridional extent similar to the linear solution of Fig. 1b and similar to numerous patterns of variability reported in previous studies for this region. By contrast, for a base point at (24°N, 60°W) in the core of the South Asian jet, Fig. 2b indicates a structure like that of Fig. 1c's linear solution: it is zonally oriented with much of the pattern confined to latitudes close to that of the base point yet extending across virtually all longitudes. Points nearly 150° of longitude away in the central North Pacific and the Gulf of Mexico achieve correlations near and above 0.60.

To determine how the contrasting structure seen in these two examples generalizes to disturbances throughout the globe, we construct one-point correlation maps for base points at each of the points on a 48 × 40 R15 transform grid. We then summarize attributes of these 1920 maps using various measures of properties that our study is concerned with. For example, to determine whether disturbances tend to be meridionally trapped when they occur near a strong jet, for each one-point correlation map we calculate the fraction of global spatial variance that occurs within 180° longitude to the east of the base point and within 10° latitude. We do this with the patterns of Figs. 1b,c and 2a,b in mind; in Figs. 1c and 2b most of the variance east of the base point is at about the same latitude as the base point while in Figs. 1b and 2a there is considerable variance at distant latitudes. Figure 3a shows this fraction plotted at the position of each base point. It indicates that the meridional trapping of the mean jet does systematically influence variability in that the fraction is more than twice as large for points near the mean jet as it is for points in low and high latitudes. This effect is especially pronounced for points that are just upstream of the main Asian and Atlantic jets.

To measure a second expected effect of the jets, namely their potential to produce patterns of variability that are longitudinally elongated, we use a different summarizing statistic. On each one-point correlation map we find the point that is farthest from the base point and that has a correlation whose absolute value is at least 0.50. Since we are interested in patterns that are zonally stretched, we measure distance in terms of longitudinal position only and plot the absolute value of the distance in Fig. 3b. Inspection of the one-point correlation charts indicates that the large values just south of the equator in Fig. 3b correspond to covariability between locations within the tropical Southern Hemisphere. Being confined to the Tropics, it is unlikely that this covariability is produced by properties of the jet. In northern midlatitudes is a band of high values that is centered on the time mean jet complex and that is flanked to the north and south by points that are only

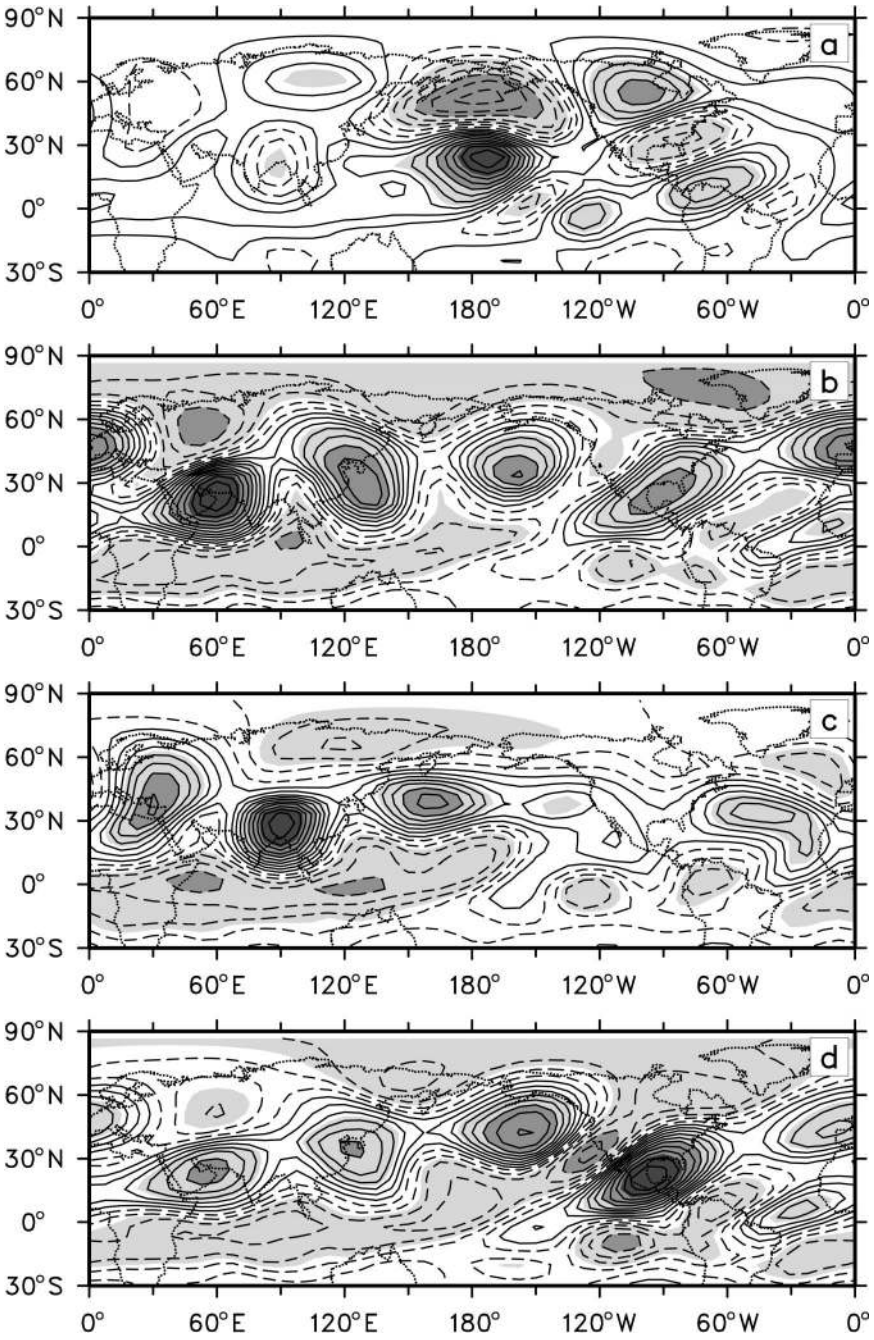

FIG. 2. One-point correlation plots of CCM3 mean DJF 300-mb streamfunction internal variability. The base point is (a) (24.4°N, 172.5°W), (b) (24.4°N, 60.0°E), (c) (28.9°N, 90°E), (d) (20.0°N, 95.5°W). Contour interval is 0.1. In this and all other figures shading is only meant to highlight high-amplitude features; it is not an indicator of statistical significance. Section 2 explains which features in the plots can be viewed with confidence. Generally speaking, plots of correlation coefficients from CCM3 have confidence intervals at the 95% level of about ± 0.05 while for observational data the confidence intervals are about ± 0.20.

teleconnected to nearby locations. Examination of the distant points that are highly correlated with base points in the jet region indicates that they too tend to be near the jet core. Thus, this figure confirms that the jetstream does influence the organization of low-frequency variability by producing zonally elongated disturbance patterns.

The statistics of Figs. 3a and 3b are not the only interesting attributes of families of one-point correlation plots. In their study of teleconnection patterns, Wallace

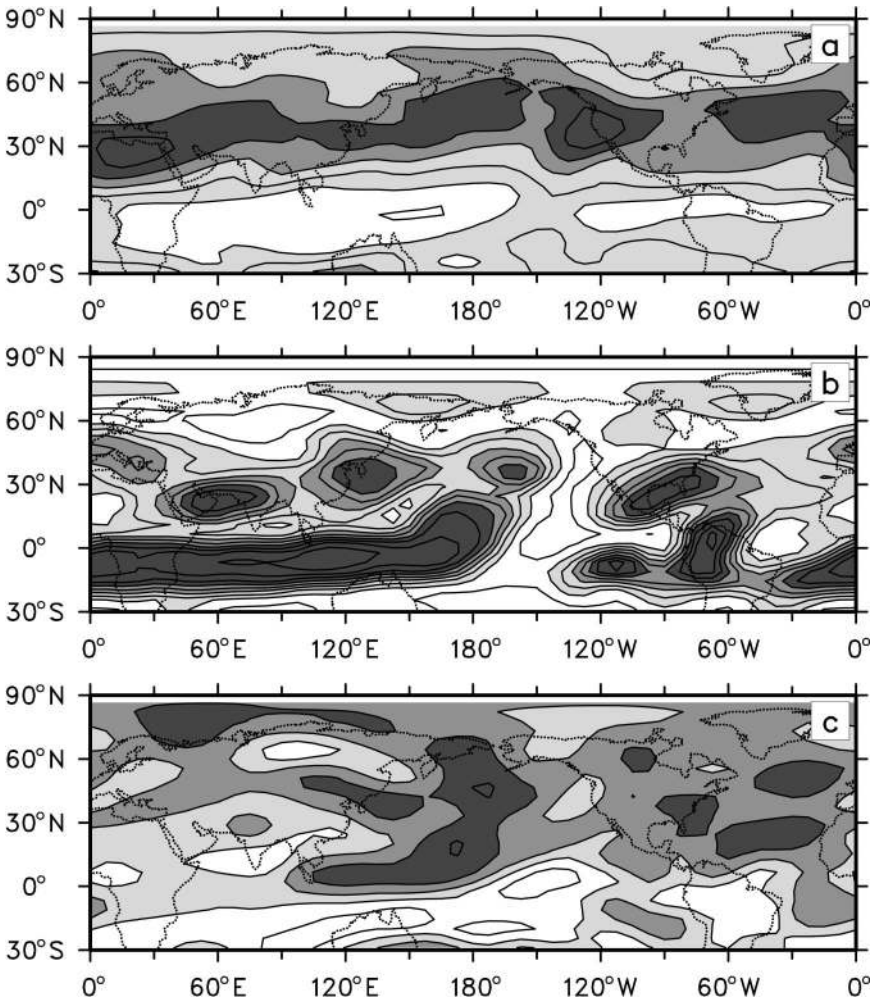

FIG. 3. Indications of the structure of one-point correlation plots with base points at locations throughout the globe and for mean DJF 300-mb streamfunction internal variability taken from CCM3. (a) The fraction of global variance in a one-point correlation plot that is within 10° lat and no more than 180° east of the base point. Contour interval is 0.1. Darkest shading begins at 0.5. (b) The longitudinal distance to that point that is farthest from the base point and that covaries with the base point with a correlation coefficient of at least 0.50. Contour interval is 2×10^6 m. Darkest shading begins at 12×10^6 m. (c) Teleconnectivity as defined by Wallace and Gutzler (1981). Contour interval is 0.1. Darkest shading begins at 0.7.

and Gutzler (1981) used another statistic of one-point correlation plots, which they called ''teleconnectivity.'' The teleconnectivity of a base point is the absolute value of the temporal correlation between the base point and that point on the globe that is most negatively correlated with the base point. Figure 3c displays the teleconnectivity for our dataset. Interestingly it gives a rather different perspective from the Fig. 3b measure as to where prominent teleconnections take place. By the conventional teleconnectivity measure South Asia is not a region with unusual connections to other regions while by our measure it is. This distinction results from our measure's emphasis on remoteness of the teleconnection, a criterion that teleconnectivity does not take into account.

Having discovered unusually distant connections between points in the jets, we are interested in the structure of the patterns that are associated with these points, so we examine some individual one-point correlation plots. We have already discussed one such plot, namely Fig. 2b's chart of covariability associated with the (24°N, 60°E) base point. Figure 2c gives the one-point correlation for another base point in the South Asian jet, (29°N, 90°E). It too indicates that variability in this region is largely trapped in the jet and consists of a pattern that covers a broad longitudinal domain, though, unlike its neighbor to the west, this base point is not associated with a pattern that completely circumscribes the globe. Within the waveguide, the pattern of variability in this plot is very similar to the pattern for the

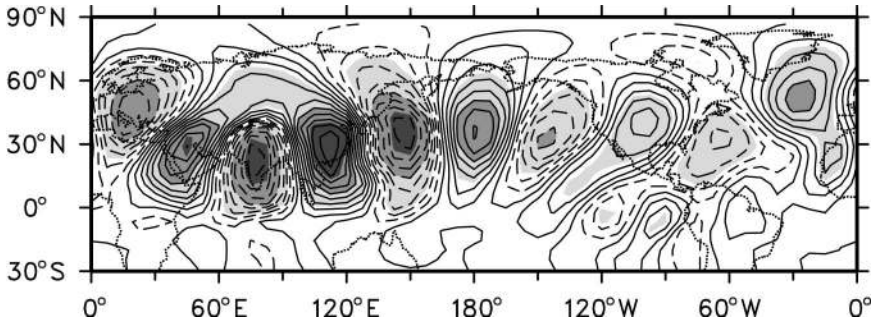

FIG. 4. One-point correlation plot for CCM3 mean Dec–Feb (DJF) 300-mb nondivergent v wind component internal variability for a base point at (28.9°N, 112.5°E). Contour interval is 0.1.

(24°N, 60°E) base point except for being shifted 30° eastward. Examination of other one-point correlation plots for base points near the South Asian mean jet indicates similar behavior. From the Gulf of Mexico eastward to near the west coast of North America, these maps all consist of roughly the same zonal wave five pattern confined to the mean jet but with a longitudinal phase that is determined by the longitude of the base point. Even the midlatitude points in Fig. 3b that have distant teleconnections but that are not in the South Asian jet are associated with similar patterns. This can be seen in Fig. 2d, which shows one such location, a base point at (20°N, 97°W). Again, a circumglobal pattern emerges.

b. Analysis of v wind

In many ways the results of the streamfunction analysis confirm the hypothesis we started with, but one aspect of it is unexpected. Each of the patterns in Figs. 2b–d has a marked quasi-zonally symmetric component. Examination of other one-point correlation plots for base points near the mean jet share this same feature. This is of interest because it may be that the distant teleconnections we have found are boosted by this component, yet its structure is not suggestive of a feature that is caused by conventional waveguide effects. For this reason we redo key aspects of our analysis of one-point correlation maps, but use the v component of the CCM3 nondivergent 300-mb wind. We choose this field because, being proportional to the zonal gradient of streamfunction, it has no zonal mean. Using v has the added attribute of being an implicit space filter that gives more weight to shorter zonal scales than does streamfunction and thus should preferentially emphasize the smaller scales that theory says should be trapped in jets.

We begin by looking at a sample one-point correlation plot. We choose a point at (29°N, 112°E), which is just upstream of the strongest part of the waveguide and is a location associated with large v anomalies in the streamfunction correlation pattern shown in Fig. 2b. As shown in Fig. 4, variability linked to this location consists of a sequence of lobes that stretch zonally along the same axis of midlatitude points with distant covariability identified in the streamfunction analysis. As expected, the pattern has no quasi-zonally symmetric component, but in spite of this, large-valued distant correlations are present, with correlations at the centers of each lobe being at least 0.40. Moreover the meridional confinement of the pattern to the vicinity of the mean jet is even more apparent in this pattern than it was for the streamfunction one-point correlation plots.

Using some of the same measures to summarize the structure of low-frequency variability of v that we used for streamfunction, we find that the influence of the mean jets is even more apparent for v. For example, Fig. 5a displays, for v, the measure of distant covariability that was shown in Fig. 3b for streamfunction. For v, all of the locations with distant teleconnections are in the vicinity of the mean jets, presumably because the use of v has removed the zonal mean perturbations that produced the large tropical values when streamfunction patterns were analyzed. On the other hand, even though teleconnectivity via zonal mean anomalies has been removed in this approach, the typical distance to covarying points is about the same for points near the mean jets as it was when streamfunction was considered. Interestingly, when we apply the conventional definition of teleconnectivity to v (Fig. 5b), the largest teleconnectivity is found in the jet stream waveguide and not in the northern ocean basins where large teleconnectivity is typically found for geopotential or streamfunction (Fig. 3c). Thus, when a variable is used that puts emphasis on intermediate scales and does not have a zonal mean component that masks upstream and downstream negative correlations (compare Figs. 4 and 2), even this measure of covariability indicates the importance of waveguide effects.[2]

[2] It may be for this same reason that Hsu and Lin (1992) found that teleconnectivity was prominent in South Asia for bandpass- but not lowpass-filtered streamfunction, bandpass filtering being an implicit spatial filter that emphasizes smaller scales and deemphasizes the zonal mean.

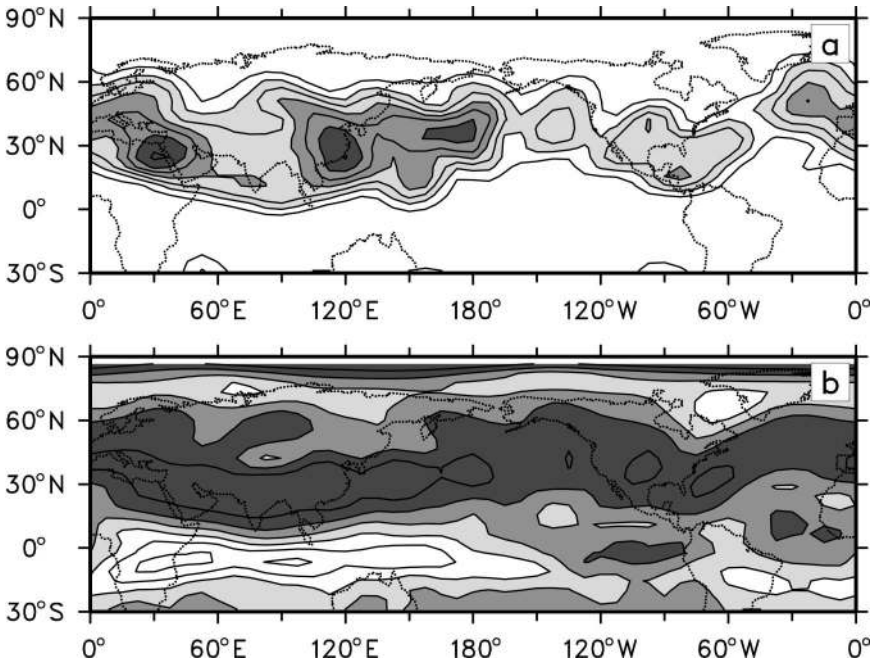

FIG. 5. Indications of the structure of one-point correlation plots with base points at locations throughout the globe and for CCM3 mean DJF 300-mb nondivergent v wind component internal variability. (a) The longitudinal distance to that point that is farthest from the base point and that covaries with the base point with a correlation coefficient of at least 0.50. Contour interval is 2 $\times 10^6$ m. (b) Teleconnectivity. Contour interval is 0.1. Shading boundaries match corresponding panels in Fig. 3.

c. The family of waveguide patterns

Examination of many one-point correlation plots of v reinforces the impression seen in Fig. 2's one-point correlation plots of streamfunction that disturbances trapped in the South Asian waveguide are different from conventional teleconnection patterns; they have no preferred longitudinal phase. To check this we perform an EOF analysis of v restricted to the region between the equator and 45°N and eastward from 0° to 120°E. Aside from being zonally shifted with respect to each other, the two leading vEOFs (Fig. 6) have nearly identical structure. Moreover, each explains a similar amount of variance (38% vs 34%). Thus together the two patterns do form a continuous family of structures, rather than two discrete patterns.

The statistic of Figs. 3b and 5a indicates that some *points* in the South Asian waveguide have more distant teleconnections than do others, but given the makeup of variability within the waveguide, it may be more accurate to say that certain *phases* of the waveguide family have more distant teleconnections than do others. As a means of verifying this we measure the strength of covariability on the opposite side of the hemisphere associated with various phases of the family of South Asian jet patterns. This can be done by considering

$$P(\phi) = v\text{EOF1} \times \cos(\phi) + v\text{EOF2} \times \sin(\phi),$$

where $\phi \in [0, 2\pi]$ represents the phase of the family of patterns and the vEOFs are the normalized sector vEOFs of Fig. 6. For each ϕ we regress global fields of model v against projections of v onto $P(\phi)$ as a means of determining the global disturbance field associated with activity in the waveguide that has phase ϕ. We then calculate the mean square of the resulting fields within sectors of interest. The ''Asian waveguide'' column of Table 1 shows the mean squares when they are calculated in the sector from 0° to 120°E of the Northern Hemisphere, where the South Asian waveguide resides. There is little dependence on ϕ. By contrast the ''Western Hemisphere'' column indicates that when the squares of the regressed fields are calculated in the sector from 180° to 60°W, the associated variability is highly dependent on the phase of the South Asian waveguide pattern. The values in this column have a maximum near $\phi = 1/8\pi$ indicating this is a special phase of South Asian waveguide activity. It has especially strong distant teleconnections.

d. A special waveguide pattern

It turns out that the global pattern associated with the special phase of the South Asian waveguide pattern is such a large part of low-frequency variability in CCM3, EOF analysis is an effective means of producing this same pattern. If we compare global vEOF1 (Fig. 7a) to the global v field regressed from projec-

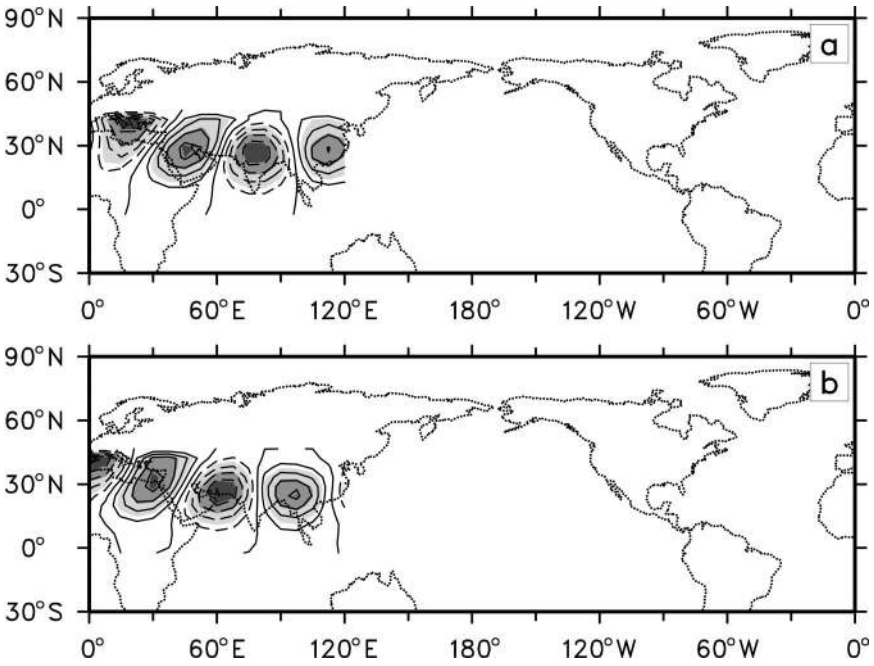

FIG. 6. The (a) leading and (b) second leading EOFs of 300-mb nondivergent v wind component for CCM3 mean DJF internal variability in the region between the equator and 45°N and eastward from 0° to 120°E. Contour interval is 0.04.

tions onto $P(1/8\pi)$ (not shown), we find the two are nearly identical. Thus global vEOF1 corresponds to that phase of the South Asian waveguide family that has the most widespread teleconnections, and we use it as a convenient means of defining this special circumglobal teleconnection pattern. Furthermore, we note that global vEOF2 (Fig. 7b) matches the structure of the quadrature pattern, $P(5/8\pi)$, and its associated global field. So together global vEOF1 and vEOF2 capture much of the variability in the South Asian waveguide together with its global covariability. Unlike for the sector vEOFs but consistent with Table 1, for these global vEOFs, the leading eigenvector explains considerably more variance than does the second leading eigenvector (22% vs 13%).

TABLE 1. Area-averaged squared CCM3 v wind component regressed from projections onto pattern $P(\phi)$ assuming $P(\phi)$ has an amplitude of 1.0. Asian waveguide refers to an average over the Northern Hemisphere region eastward from 0° to 120°E. Western Hemisphere refers to an average over the Northern Hemisphere region eastward from 180° to 60°W. Units are 0.001 $m^2\ s^{-2}$.

ϕ	Asian waveguide	Western Hemisphere
0π	6.44	2.47
$1/8\pi$	6.42	2.55
$1/4\pi$	6.29	2.20
$3/8\pi$	6.08	1.54
$1/2\pi$	5.94	0.97
$5/8\pi$	6.01	0.96
$3/4\pi$	6.20	1.45
$7/8\pi$	6.36	2.06

To establish a link between the circumglobal pattern and our streamfunction results, we find the 300-mb streamfunction anomalies that are associated with global vEOF1 by regressing DJF streamfunction from the principal components of global vEOF1. The 300-mb streamfunction field that results is depicted in Fig. 8a. It corresponds to the amplitude of this field when the predictor has a value of one standard deviation. We note that the prominent lobes of this pattern over southern Europe, the Arabian Sea, the Korean Peninsula, Hawaii, and just north of the Gulf of Mexico exactly match the locations of especially strong distant teleconnectivity in Fig. 3b, further evidence that vEOF1 captures the waveguide pattern associated with the strongest widely spaced covariability. Consistent with this, it also matches the one-point streamfunction correlation plots we have previously displayed for base points at two of these locations (Figs. 2b and 2d).

In addition to clarifying the connection between locations of especially distant streamfunction- and v covariability, the streamfunction anomalies of Fig. 8a are also useful for addressing another issue. We remarked that the strong quasi-zonally symmetric components of waveguide patterns in Figs. 2b–d were not expected from the linear waveguide solution of the introduction. For this reason it is of interest to determine whether this component is actually temporally independent from the wavy components of those patterns. Figure 8a's regressed streamfunction helps determine this because global vEOF1 represents only the wavy component. The

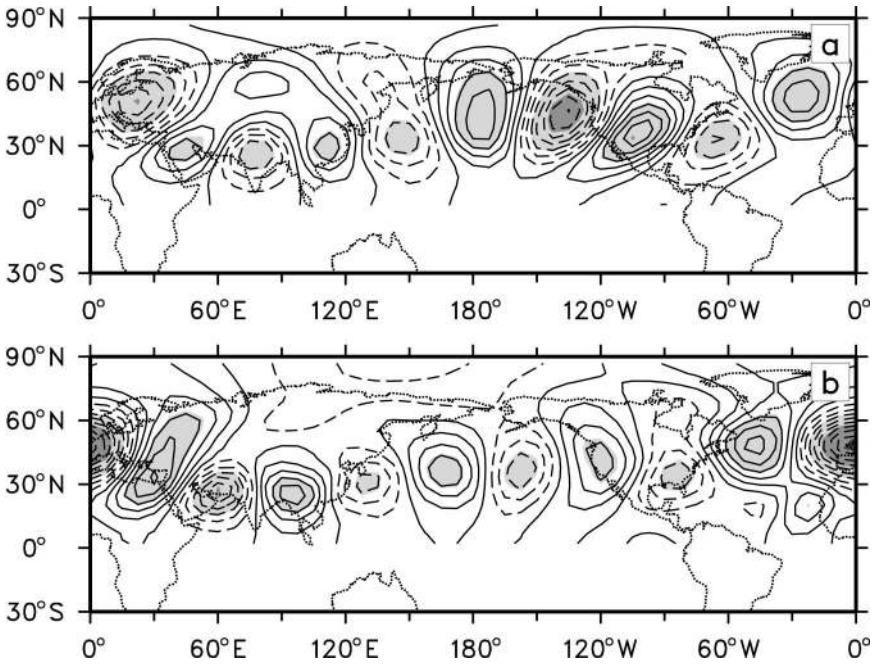

FIG. 7. The (a) leading and (b) second leading EOFs of Northern Hemisphere 300-mb nondivergent v wind component for CCM3 mean DJF internal variability.

fact that the lobes of one sign in this figure are stronger than the lobes of the opposite sign, then, indicates that the wavy component of this dominant pattern is associated with zonal mean variability. On the other hand the zonal mean of regressed streamfunction is not nearly as strong as the zonal mean of Fig. 2's one-point correlation plots. We would expect this same outcome of much stronger zonal symmetries in a streamfunction (or

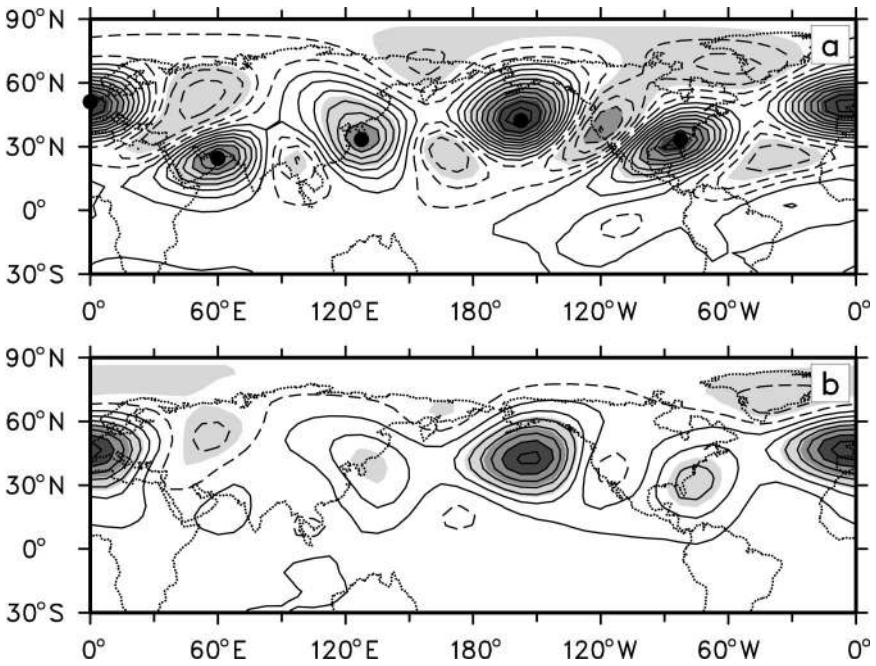

FIG. 8. Fields predicted by a one standard deviation anomaly in the principal component for the leading EOF of CCM3 mean DJF 300-mb nondivergent v as given by linear regression. (a) 300-mb streamfunction. Contour interval is 5×10^5 m^2 s^{-1}. (b) 850-mb streamfunction. Contour interval is 5×10^5 m^2 s^{-1}.

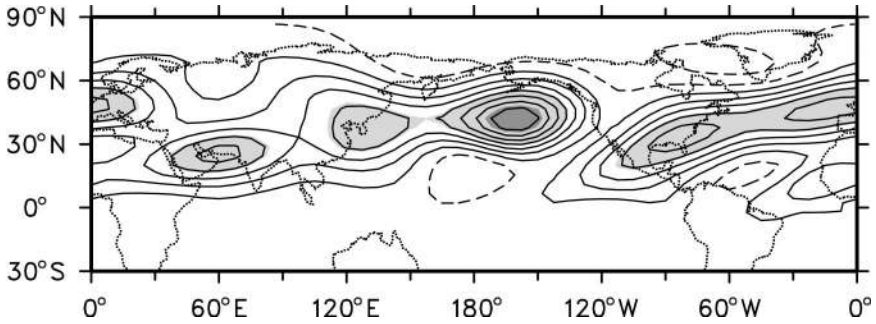

FIG. 9. The leading EOF of Northern Hemisphere 300-mb streamfunction for CCM3 mean DJF internal variability.

geopotential) keyed analysis than a v keyed analysis if we were observing a system with two, independent modes, one largely annular and the other primarily wavy. Thus, since the streamfunction based analysis appears to be mixing two phenomena, we take the pattern of v regressed Fig. 8a as the more fundamental streamfunction representation of the dominant circumglobal waveguide pattern.

To produce a more complete picture of this recurring circulation pattern, we learn about its vertical structure by regressing CCM3 DJF 850-, 700-, and 500-mb streamfunction anomalies against projections onto vEOF1. Consistent with the behavior commonly associated with interannual variability (Blackmon et al. 1979), the results indicate that the pattern is equivalent barotropic everywhere though anomalies over central Asia and central North America virtually disappear near the surface as can be seen in Fig. 8b's depiction of the regressed 850-mb streamfunction field.

e. Manifestations

Having found that the signature of jet stream–trapped covariability between widely spaced points in the Northern Hemisphere during winter is quite prominent, it seems possible that this mechanism may influence other prominent low-frequency phenomena without having been recognized in the past. We consider two prevalent patterns of CCM3 low-frequency variability.

The first pattern that we consider is simply the leading EOF of Northern Hemisphere DJF mean 300-mb streamfunction. Shown in Fig. 9, this pattern explains 22% of the model's internal variability. The fact that the dominant waveguide pattern we have documented is embedded in this EOF is clear; the five local maxima of its structure are in exactly the same locations as the centers of the waveguide pattern (Fig. 8a). Further evidence of the connection between this streamfunction EOF and the circumglobal waveguide pattern comes from finding that its principal component is correlated with the principal component of global vEOF1 by a value of 0.96. Consistent with our streamfunction one-point correlation results, the streamfunction EOF1 analysis does embellish the quasi-zonally symmetric component of the streamfunction pattern associated with the waveguide pattern, but a similar analysis to that carried out in section 3c indicates that this enhancement probably results from mixing two physical phenomena that are actually temporally independent. (That is, if one regresses streamfunction from an index consisting of projections of v onto the v field nondivergently derived from ψEOF1, much of the zonal component of ψEOF1 disappears.)

The second pattern that we consider is the North Atlantic Oscillation (NAO). We do this because the circulation anomalies that are associated with the Atlantic portion of the leading circumglobal teleconnection pattern are reminiscent of the NAO (Hurrell 1995). To determine the structure of the NAO in our CCM3 climate, we use a straightforward index, namely the leading EOF of 850-mb streamfunction in the North Atlantic sector. If we restrict ourselves to the domain between 90°W and 30°E in the Northern Hemisphere and find the leading EOF of DJF means, we get the pattern shown in Fig. 10a. This EOF explains 47% of the sector variance. The similarity of this pattern to analyses of fields from nature by Hurrell (1995) indicates that within this sector CCM3 develops variability much like nature's NAO, even for the fields of internal variability we are studying.

To see whether there is any connection between this pattern and the circumglobal pattern, in Fig. 10b we display Northern Hemisphere 300-mb streamfunction correlated with the principal component of the 850-mb streamfunction sector EOF1. In addition to the North Atlantic circulation anomalies one would expect by assuming an equivalent barotropic structure, in CCM3 our NAO index is associated with perturbations over the entire Northern Hemisphere. Centers of correlation with values greater than 0.50 exist in every quadrant of the hemisphere. Unlike in the rest of our investigation we have chosen to display results related to the NAO on polar stereographic projections so they can easily be compared to earlier studies. To make it apparent that the circumglobal anomalies in Fig. 10b are virtually identical to the anomalies of the circumglobal pattern

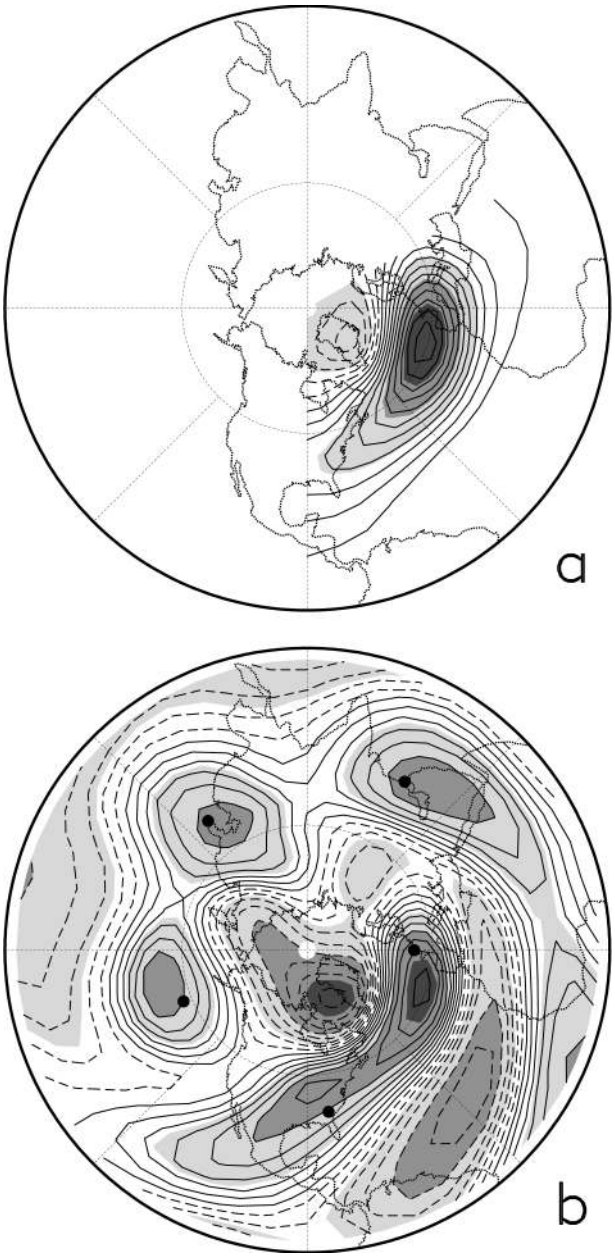

FIG. 10. (a) Leading EOF of CCM3 mean DJF 850-mb streamfunction internal variability for the Northern Hemisphere sector between 90°W and 30°E. (b) Correlation of CCM3 mean DJF 300-mb streamfunction internal variability with the principal component associated with the EOF of (a). The five heavy dots mark the centers of the five lobes in the streamfunction plot of Fig. 8a. Contour interval is 0.1.

we have been studying, the locations of the five prominent lobes in the circumglobal pattern from Fig. 8a are marked by dots on Fig. 10b. Clearly the 300-mb NAO anomalies and the circumglobal pattern have these features as well as the distinct annular feature in common. Hence for CCM3 any analysis of the NAO is likely to include contributions from the circumglobal waveguide pattern.

f. Robustness

As explained in section 2 we can have a great deal of confidence in the correlation coefficients that our analysis of CCM3 is based on. But this fact says nothing about the confidence we can have in the realism of the features we have identified. As one step toward ruling out the possibility that our results are an artifact of the model's formulation, we repeat most of our analysis for the NSIPP GCM described in section 2. We find that each of the characteristics we have found for CCM3 carries over to this second model. As an indication of this similarity, we show in Fig. 11 the distance to the farthest point for which the covariability of DJF 300-mb streamfunction has a correlation coefficient whose absolute value is at least 0.50. Though the distances in this plot are somewhat smaller than in Fig. 3b's corresponding map for CCM3, the geographical distribution of distances is very similar. In midlatitudes the greatest distances occur for points near the mean jets and within these regions there are local maxima at virtually the same longitudes found for CCM3. From this and other results from our analysis of the NSIPP model, we conclude that there is nothing unusual about CCM3's formulation that is producing the waveguide effects we have investigated.

4. Results from nature

We now turn to the reanalysis dataset described in section 2 to investigate whether the effects of the mean jet can be detected there too. Recall from section 2 that in this section we will largely rely on similarities with our results for the GCM ensembles to establish confidence in our findings.

We begin as we did with the GCM data by determining whether patterns of variability near the South Asian mean jet are more zonally elongated than are patterns in the central North Pacific. Picking base points in the same locations that we used in Figs. 2a,b, we find the same distinctions for nature's variability that we found in the GCM. The North Pacific pattern (Fig. 12a) is an arch, while the South Asian pattern (Fig. 12b) is much more confined in the meridional direction and stretches out in the zonal direction. If we had not seen similar patterns in the GCMs, we might not have much confidence in the South Asian pattern, but given the GCM results we find the zonal character of the pattern compelling.

Next we see how these results generalize to points throughout the Northern Hemisphere by using two of the same statistics that we applied to GCM anomalies. Figure 13a deals with streamfunction and depicts the longitudinal distance to the most distant point that covaries with a correlation coefficient of at least 0.40. For the GCMs we used a criterion of 0.50 for the corresponding calculation, but in nature points that meet that cutoff are somewhat closer to base points. Aside from

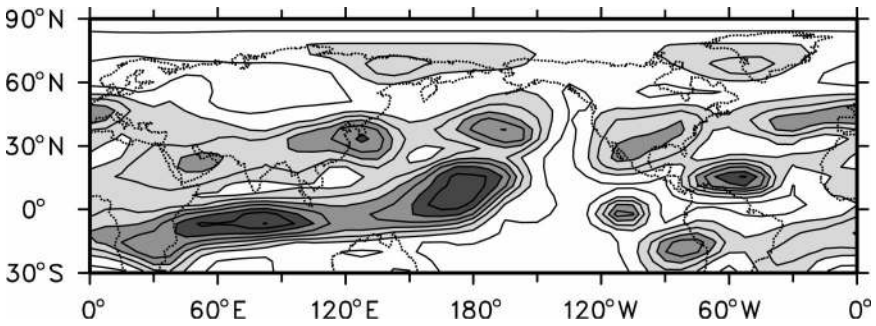

FIG. 11. Same as 3b except NSIPP GCM data are used.

this distinction, the figure shows that the features we saw in the GCMs are also present in nature. Points along the South Asian jet and off the east coast of North America are more strongly connected to distant points than are other Northern Hemisphere midlatitude points. Some of these locations covary with locations that are especially great distances away. The position of these special locations is shifted a bit in nature from their positions in the GCM, especially near the east coast of North America, but their spacing is similar. Figure 13b displays Wallace and Gutzler's (1981) conventional measure of teleconnectivity applied to v, and again we find that nature behaves much like CCM3 (Fig. 5b). Not only are the points with largest teleconnectivity confined to the waveguide band, but even many of the local maxima within that band match those in CCM3. Of course we know from Wallace and Gutzler (1981) and Hsu and Lin (1992) that, just as we found with the GCM datasets, if we calculate teleconnectivity for nature's low-frequency streamfunction or geopotential the mean jets are not regions of especially prominent connectivity.

One of the interesting aspects of jet-trapped variability in CCM3 is that it has a preferred zonal scale and no preferred phase within the South Asian jet. To see if these characteristics carry over to nature, we again perform an EOF analysis of the v field within the South Asian sector and find (Fig. 14) that together the leading EOFs describe a family of patterns that are nearly identical to the family in CCM3. As listed in Table 2, we also find that for one phase of this family, variability within the waveguide is more strongly related to variability on the other side of the hemisphere than for other

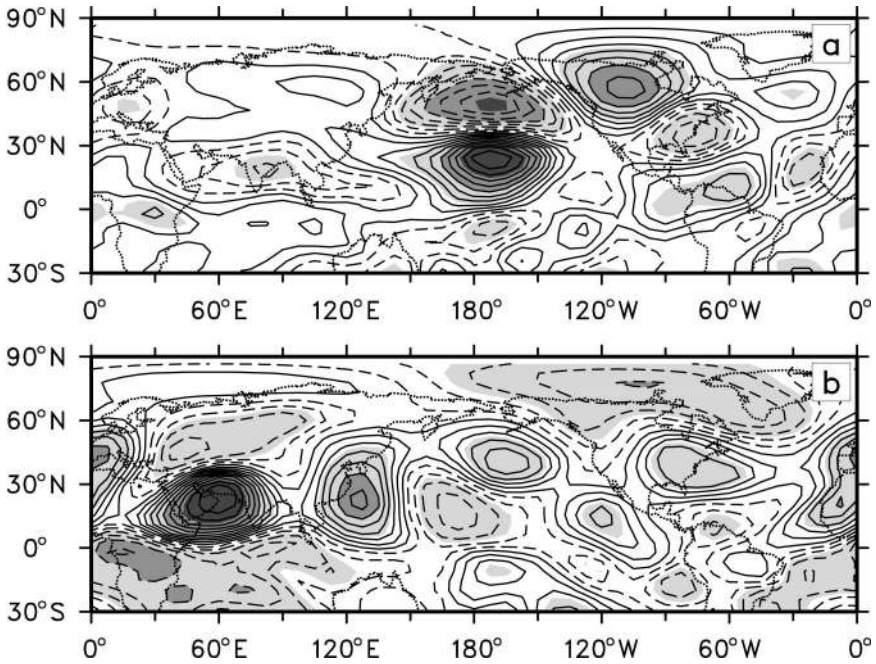

FIG. 12. One-point correlation plots of observed monthly mean DJF 300-mb streamfunction departures from centered 3-month averages. The base point is (a) (24.4°N, 172.5°W), (b) (24.4°N, 60.0°E). Contour interval is 0.1.

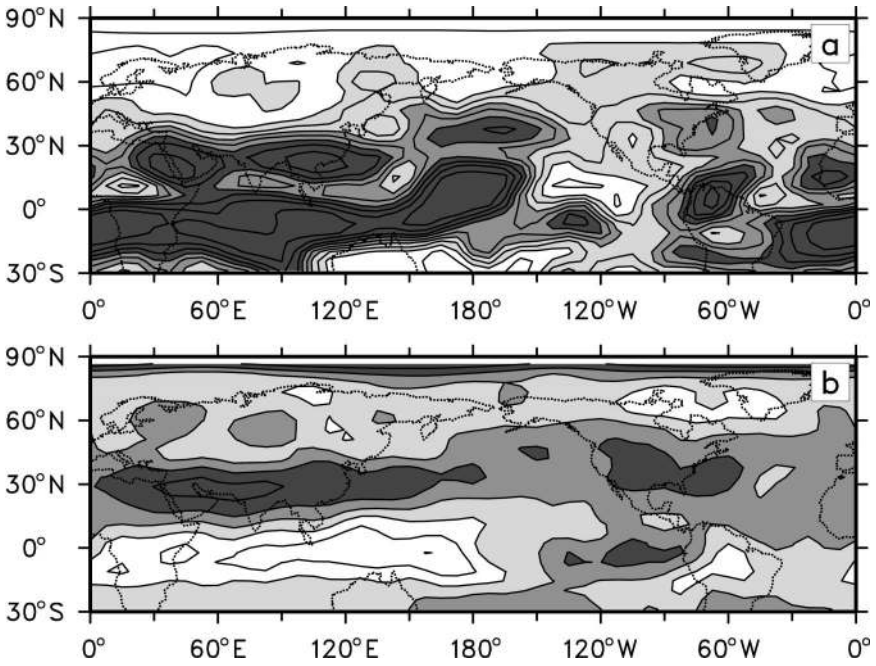

FIG. 13. Indications of the structure of one-point correlation plots with base points at locations throughout the globe and for observed monthly mean DJF departures from centered 3-month averages. (a) The same measure of covariability distance used in Figs. 3b and 11. Contour interval is 2×10^6 m. (b) Teleconnectivity for 300-mb nondivergent v component of the wind. Contour interval is 0.1. Shading boundaries match corresponding panels in Fig. 3.

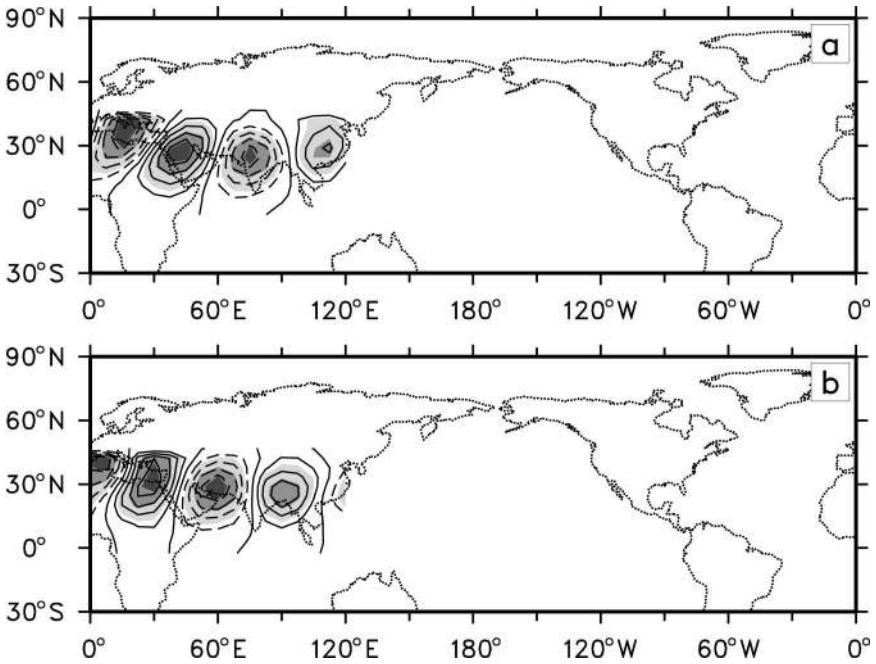

FIG. 14. The (a) leading and (b) second leading EOFs of 300-mb nondivergent v wind component for observed monthly mean DJF departures from centered 3-month averages in the region between the equator and 45°N and eastward from 0° to 120°E. Contour interval is 0.04.

TABLE 2. Same as Table 1 except data and patterns $P(\phi)$ are based on reanalysis data from nature.

ϕ	Asian waveguide	Western Hemisphere
0π	5.40	0.97
$1/8\pi$	5.23	1.03
$1/4\pi$	5.16	1.15
$3/8\pi$	5.19	1.25
$1/2\pi$	5.55	1.24
$5/8\pi$	5.96	1.14
$3/4\pi$	6.01	1.03
$7/8\pi$	5.71	0.97

phases. Further examination reveals that this phase has wave crests that are shifted about 15° longitude westward from the locations that result in maximum circumglobal teleconnections in CCM3. One apparent difference between nature and the GCM is that within the South Asian waveguide nature appears to have a favored phase in that sector vEOF1 has a larger eigenvalue (37%) than vEOF2 (26%). On the other hand this may be a result of sampling deficiencies since redoing the analysis with overlapping 30-day means reduces the eigenvalue gap.

For CCM3 the circumglobal waveguide pattern was prominent enough that it showed up as a component of the leading EOFs of streamfunction and v. We perform the corresponding EOF analyses for nature and find the same holds true. For example, Fig. 15 shows the leading EOF of monthly 300-mb streamfunction. We see that because of the strong covariability of points within the waveguide, particularly at 50°E, 110°E, 170°W, 60°W, and 0°E, these show up as maxima in this pattern. Modified versions of this calculation indicate that the details of the analysis matter and probably explain why these features have not been singled out as being special in other studies. The use of streamfunction rather than geopotential and the use of departures from season means is important.

The leading EOFs of global v from nature (not shown) also capture the same behavior seen in Fig. 7's plots of CCM3's leading global vEOFs with both showing a distinct zonal wave five pattern that is latitudinally confined to the same meandering zone of latitudes seen throughout this study. These EOFs, however, do put more emphasis on the eastern half of the Pacific and North America than is seen in their GCM counterparts, perhaps because the approximate method used to remove the effect of interannually varying SSTs leads to a larger El Niño influence in this region.

As a final test of the applicability of the CCM3 results to nature, we consider whether the waveguide behavior may be influencing studies of Northern Hemisphere circulation associated with the NAO. Proceeding as before, we form an NAO index by finding the leading EOF of 850-mb streamfunction confined to the Atlantic sector (Fig. 16a) and use the resulting principal component time series as an index. Then if we correlate 300-mb streamfunction with the variability of this index, we find the pattern in Fig. 16b. We see that in midlatitudes the zonally symmetric character of the NAO is very pronounced. In contrast to Deser's (2000) study, this rendition of the circulation associated with an NAO index tends to support Thompson and Wallace's (1998) interpretation that the NAO is actually a local analysis of a hemispheric wide mode. Second, we notice that in addition to the zonally symmetric features the circulation associated with the NAO has some strong asymmetries and the centers of those asymmetries are near the centers of the dominant waveguide pattern of our study. From this result it appears that in nature just as in CCM3, studies of the NAO (or the Arctic Oscillation) can automatically incorporate the global waveguide pattern.

Since other studies have not found such distinct nonannular centers of NAO covariability outside of the Atlantic sector, we investigate this lack of agreement and find three important contributing factors. One is our use of streamfunction as an indicator of global NAO associations. Streamfunction enhances signals in low latitudes, where the waveguide largely resides. Another factor is our use of 300 mb as the level for searching for global relationships. As seen in Fig. 8b, the waveguide patterns tend to vanish at low levels over continents so they are less likely to be detected in near surface fields. The third factor is our use of 850-mb streamfunction rather than sea level pressure when forming a

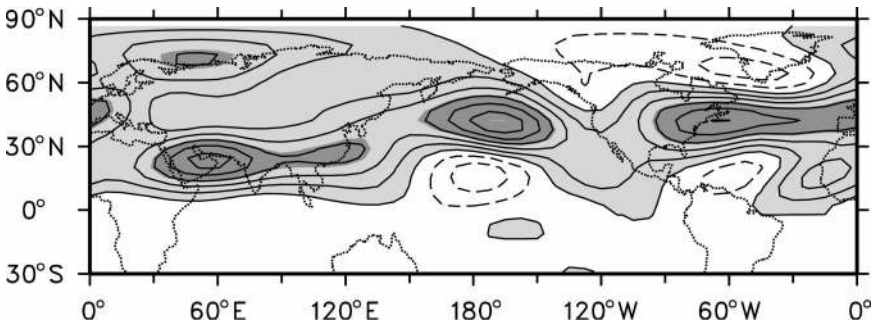

FIG. 15. The leading EOF of Northern Hemisphere 300-mb streamfunction for observed monthly mean DJF departures from centered 3-month means.

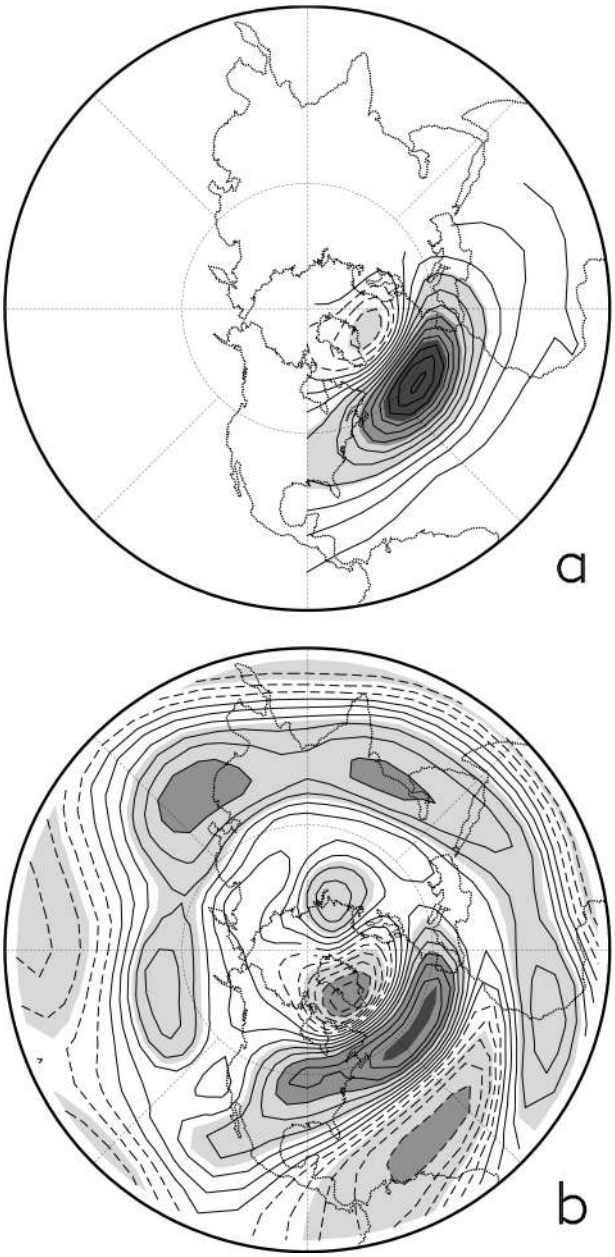

FIG. 16. Same as Fig. 10 except for observed monthly mean DJF departures from centered 3-month means.

NAO index. Streamfunction gives greater weight to the midlatitude lobe of the NAO, a feature that is a prominent component of the global waveguide pattern.

5. Summary and discussion

Our study set out to determine whether low-frequency variability is predominantly composed of patterns with pronounced meridional orientations, as one might conclude from many studies of Northern Hemisphere winter behavior, or whether there are also patterns that are primarily zonally oriented corresponding to covariability at widely separated longitudinal positions. We wondered this because solutions of the barotropic vorticity equation linearized about the climatological winter state indicate the jets act as waveguides. This means that steady solutions that are within the latitudes of the time average tropospheric jets tend to be meridionally trapped and longitudinally elongated unlike solutions forced in regions with weak meridional gradients of background vorticity. By examining the internal variability of ensembles of GCM integrations and of 39 winters of fields from nature, we have come to the conclusion that indeed the mean jet complexes do impress on low-frequency variability the structure suggested by the linear theory. In particular our investigation has found indications of the following behavior in both GCMs and nature:

1) Patterns of upper-tropospheric variability near the time mean jets tend to be meridionally confined to the vicinity of the jets and to consist of anomalies organized in chains that stretch out in the zonal direction. Associated with these patterns are points that are as much as 150° longitude apart and whose correlation coefficient of covariability is as large as 0.60 in the GCMs. This behavior is distinct from what is found in the mid North Pacific where the jet is weak and where disturbances tend to be arch shaped and thus have prominent meridional structure but much more limited zonal extent.
2) Disturbances that are trapped in the South Asian jet stream waveguide do not have preferred longitudinal phases within the waveguide and are composed primarily of zonal wavenumber 5. From this perspective the waveguide patterns can be thought of as constituting a family of structures.
3) From a global perspective these waveguide disturbances do have a preferred phase. For one phase the regions with which they covary are especially widespread and in fact essentially circumscribe the Northern Hemisphere. From this point of view the waveguide effects are responsible for the existence of a special pattern that connects all longitudes of the hemisphere, a pattern that we have referred to as the circumglobal waveguide pattern. This finding suggests that in general it is not a good idea to consider sectors when studying low-frequency phenomena.
4) Judging from the behavior of the most prominent waveguide pattern, the waveguide features are equivalent barotropic though over continents they do not extend to the lower troposphere.
5) When analyzed from fields that can have a substantial zonal mean (like geopotential or streamfunction), waveguide patterns have a nontrivial zonal mean component. This means that they are not orthogonal to annular features and are often combined with annular patterns in EOF analyses.
6) The circumglobal waveguide pattern is so prominent that its features make substantial contributions to the

leading EOF of Northern Hemisphere streamfunction variability, and it is the leading EOF of nondivergent v variability.

7) The circumglobal waveguide pattern has a distinct north–south dipole structure in the North Atlantic sector. This means that it projects onto NAO indices and its features contribute to variability at locations throughout Northern Hemisphere midlatitudes that are associated with NAO variability. When an NAO index that emphasizes North Atlantic midlatitudes is used, at 300 mb these locations have a correlation coefficient of covariability with the NAO of more than 0.50.

Though our study supports the qualitative distinctions between low-frequency midlatitude variability in a mean jet and in a region with more uniform background gradients predicted by linear theory, there are some aspects of the structures we have analyzed that a theory based on slow variations in the background state is not so successful at explaining. One such characteristic is the fact that the global character of patterns associated with variability in the South Asian waveguide depends on the longitudinal phase of the South Asian portion of the disturbance. Our results suggest that in one phase (Fig. 2b) the waveguide disturbances are associated with a PNA-like arching pattern across North America while in the quadrature phase (Fig. 2c) they are not. Recalling that studies (e.g., Simmons et al. 1983) of the normal modes of the barotropic vorticity equation linearized about boreal winter conditions indicate the system may have near resonant, geographically fixed, modes similar to this arching pattern, one interpretation of this result is that in one phase the waveguide features excite such a mode so that together they span the globe, while in the quadrature phase they do not and the pattern dissipates in the central Pacific.

Another feature that traditional waveguide theory as presented does not explain is the apparent concurrence of waveguide-like features and distinct zonal mean anomalies. We have found that the zonally symmetric component of such patterns can be artificially emphasized if one-point correlation or EOF analyses are applied to fields whose variability includes prominent zonal mean features, but we have also concluded that variability in the waveguide does have a genuine zonal mean. We do not know the cause of this inherent feature, but we point out that new theories may not need to be developed to explain this result. The simplest explanation may simply be that at a given latitude localized divergence anomalies can have a zonal mean component. These then can act to force disturbances with both wavelike and zonal mean components. Indeed, in their linear modeling study, Hoskins and Ambrizzi (1993) showed (their Fig. 7) that a vorticity source (which included a zonal mean) placed at (40°N, 75°W) would excite a pattern rather like the circumglobal pattern we have identified, including a zonally symmetric component. In fact even the zonal mean component of the forcing may not be crucial in such a calculation. Branstator (1985) found that the leading normal mode of a GCM's wintertime state had a very long period and a distinct zonal mean in midlatitudes, yet because this mode is nearly neutral it would only take minimal forcing to excite. Thus anything that excites the series of highs and lows usually expected to occur in the waveguide might also excite such a disturbance.

We believe that our finding that NAO and AO indices are keyed to North Atlantic features that resemble the circumglobal waveguide pattern identified in our study may have some bearing on why studies of the Arctic Oscillation tend to include a center of variability in the central North Pacific; the North Atlantic and North Pacific are two of the five lobes of the circumglobal pattern (and the two that penetrate to the surface). But without further analysis we are not certain whether the NAO and AO and the circumglobal pattern are physically linked or whether they just happen to have similar structure in the North Atlantic.

Finally, we need to point out that though our study has intentionally factored out the influence of interannually varying SSTs on the low-frequency patterns we have investigated, this is not meant to imply that the patterns we have found do not play a role in the reaction of the atmosphere to such SSTs. In fact from the fluctuation–dissipation theorem, one might expect that they *would* influence how the atmosphere reacts to SSTs. Preliminary results from a study of precipitation associated with the circumglobal waveguide pattern indicate that it is accompanied by substantial tropical rainfall anomalies in both nature and GCMs. But until further analysis is done it is not clear whether these precipitation anomalies force the waveguide pattern or owe their existence to that pattern. Less ambiguous is the recent work by Chen (2002) who has found that tropical Pacific cold events are accompanied not only by circulation anomalies with the familiar arching structure over the northeast Pacific and North America but also by a series of smaller scale highs and lows that stretch across South Asia in the waveguide.

Acknowledgments. The author is grateful to T.-C. Chen for sharing preliminary results from his study of tropical Pacific cold events, which provided the initial motivation for this work. He has benefited from comments on an earlier version of this manuscript that were provided by Saravanan, Judith Berner, and Kevin Trenberth. Discussions of this investigation with these same individuals as well as with Jim Hurrell, Jeff Anderson, and Zoltan Toth have also helped crystalize some of its ideas. Andy Mai prepared the datasets and produced the figures. This project was partially funded by Grant NA16GP1015 from NOAA's Office of Global Programs and by Grant S-10180-X from NASA's Seasonal-to-Interannual Prediction Project.

APPENDIX

Correlation Coefficient Confidence Intervals

As explained in basic statistics books like Anderson (1971), to assess the confidence of correlations, one must transform the correlation estimates using Fisher's *z* transformation. Once that is done they are expected to have normal distributions, and standard techniques using the *t* statistic can be used to derive confidence intervals, whose width turns out to be a function of the value of the estimated correlation. Determining the number of temporal degrees of freedom in the samples used in our study is not straightforward, but for the sake of argument assume that our observational record contains 78 independent samples. This number is arrived at by assuming each 3-month winter contains two samples. Then if one wants to achieve a confidence of 95%, one can determine only values of the correlation to within an interval that is about 0.4 wide. For example, if the best estimate is that the correlation coefficient is zero, then the 95% confidence interval is (−0.23, 0.23), while if the best estimate is that the correlation coefficient is 0.50, then the confidence interval is (0.31, 0.65). By contrast with our CCM3 ensemble of 22 members each consisting of 44 seasonal averages, the 95% confidence interval for a correlation estimate of zero is (−0.06, 0.06) and for an estimate of 0.50 it is (0.45, 0.55), assuming each seasonal mean is independent. Likewise, for the NSIPP ensemble, the 95% confidence interval for an estimate of zero is (−0.10, 0.10) while for an estimate of 0.50 it is (0.42, 0.57).

REFERENCES

Ambrizzi, T., B. J. Hoskins, and H.-H. Hsu, 1995: Rossby wave propagation and teleconnection patterns in the austral winter. *J. Atmos. Sci.,* **52,** 3661–3672.

Anderson, T. W., 1971: *The Statistical Analysis of Time Series.* John Wiley and Sons, 704 pp.

Bacmeister, J., P. J. Pegion, S. D. Schubert, and M. J. Suarez, 2000: Atlas of seasonal means simulated by the NSIPP 1 atmospheric GCM. Vol. 17. NASA/TM-2000-104505, 208 pp.

Barnston, A. G., and R. E. Livezey, 1987: Classification, seasonality and persistence of low-frequency atmospheric circulation patterns. *Mon. Wea. Rev.,* **115,** 1083–1126.

Blackmon, M. L., 1976: A climatological spectral study of the 500 mb geopotential height of the Northern Hemisphere. *J. Atmos. Sci.,* **33,** 1607–1623.

——, R. A. Madden, J. M. Wallace, and D. S. Gutzler, 1979: Geographical variations in the vertical structure of geopotential height fluctuations. *J. Atmos. Sci.,* **36,** 2450–2466.

Branstator, G., 1983: Horizontal energy propagation in a barotropic atmosphere with meridional and zonal structure. *J. Atmos. Sci.,* **40,** 1689–1708.

——, 1985: Analysis of general circulation model sea surface temperature anomalies using a linear model. II: Eigenanalysis. *J. Atmos. Sci.,* **42,** 2242–2254.

Chen, T.-C., 2002: A North Pacific short-wave train during the extreme phases of ENSO. *J. Climate,* in press.

Deser, C., 2000: On the teleconnectivity of the ''Arctic Oscillation.'' *Geophys. Res. Lett.,* **27,** 779–782.

Hack, J. J., J. T. Kiehl, and J. W. Hurrell, 1998: The hydrological and thermodynamic characteristics of the NCAR CCM3. *J. Climate,* **11,** 1179–1206.

Horel, J. D., 1981: A rotated principal component analysis of the interannual variability of the Northern Hemisphere 500 mb height field. *Mon. Wea. Rev.,* **109,** 2080–2092.

Hoskins, B. J., and D. Karoly, 1981: The steady, linear response of a spherical atmosphere to thermal and orographic forcing. *J. Atmos. Sci.,* **38,** 1179–1196.

——, and T. Ambrizzi, 1993: Rossby wave propagation on a realistic longitudinally varying flow. *J. Atmos. Sci.,* **50,** 1661–1671.

——, A. J. Simmons, and D. C. Andrews, 1977: Energy dispersion in a barotropic atmosphere. *Quart. J. Roy. Meteor. Soc.,* **103,** 553–567.

Hsu, H.-H., and S.-H. Lin, 1992: Global teleconnections in the 250-mb streamfunction field during the Northern Hemisphere winter. *Mon. Wea. Rev.,* **120,** 1169–1190.

Hurrell, J. W., 1995: Decadal trends in the North Atlantic Oscillation: Regional temperatures and precipitation. *Science,* **269,** 676–679.

Hurrell, J. W., and K. E. Trenberth, 1999: Global sea surface temperature analyses: Multiple problems and their implications for climate analysis, modeling, and reanalysis. *Bull. Amer. Meteor. Soc.,* **80,** 2661–2678.

——, J. J. Hack, B. A. Boville, D. L. Williamson, and J. T. Kiehl, 1998: The dynamical simulation of the NCAR Community Climate Model version 3 (CCM 3). *J. Climate,* **11,** 1207–1236.

Kalnay, E., and Coauthors, 1996: The NCEP/NCAR 40-Year Reanalysis Project. *Bull. Amer. Meteor. Soc.,* **77,** 437–471.

Kiehl, J. T., J. J. Hack, G. B. Bonan, B. A. Boville, D. L. Williamson, and P. J. Rasch, 1998: The National Center for Atmospheric Research Community Climate Model: CCM3. *J. Climate,* **11,** 1131–1149.

Kiladis, G. N., and K. M. Weickmann, 1992: Circulation anomalies associated with tropical convection during northern winter. *Mon. Wea. Rev.,* **120,** 1900–1923.

Kimoto, M., and M. Ghil, 1993: Multiple flow regimes in the Northern Hemisphere winter. Part I: Methodology and hemispheric regimes. *J. Atmos. Sci.,* **50,** 2625–2643.

Leith, C. E., 1978: Predictability of climate. *Nature,* **276,** 352–355.

Longuet-Higgins, M. S., 1964: Planetary waves on a rotating sphere, I. *Proc. Roy. Soc. London,* **279,** 446–473.

——, 1965: Planetary waves on a rotating sphere, II. *Proc. Roy. Soc. London,* **284,** 40–68.

Rayner, N. A., E. B. Horton, D. E. Parker, C. K. Folland, and R. B. Hacket, 1996: Version 2.2 of the Global Sea-Ice and Sea Surface Temperature data set, 1903–1994. CRTN 74, 21 pp. plus figures. [Available from Hadley Centre for Climate Prediction and Research, Met Office, London Road, Bracknell, Berkshire RG12 2SY, United Kingdom.]

Reynolds, R. W., and T. M. Smith, 1994: Improved global sea surface temperature analyses using optimum interpolation. *J. Climate,* **7,** 929–948.

Simmons, A. J., J. M. Wallace, and G. W. Branstator, 1983: Barotropic wave propagation and instability, and atmospheric teleconnection patterns. *J. Atmos. Sci.,* **40,** 1363–1392.

Smith, T. M., R. W. Reynolds, R. E. Livezey, and D. C. Stokes, 1996: Reconstruction of historical sea surface temperatures using empirical orthogonal functions. *J. Climate,* **9,** 1403–1420.

Thompson, D. W. J., and J. M. Wallace, 1998: The Arctic Oscillation signature in the wintertime geopotential height and temperature fields. *Geophys. Res. Lett.,* **25,** 1297–1300.

Walker, G. T., and E. W. Bliss, 1932: World Weather V. *Mem. Roy. Meteor. Soc.,* **4,** 53–84.

Wallace, J. M., and D. S. Gutzler, 1981: Teleconnections in the geopotential height field during the Northern Hemisphere winter. *Mon. Wea. Rev.,* **109,** 784–812.